STRENGTH OF ADHESIVE BONDED COMPOSITE LAP SHEAR JOINTS WITH AND WITHOUT EMBEDDED CRACKS

Liyong Tong

Department of Aeronautical Engineering, University of Sydney, NSW 2006, Australia

SUMMARY: An experimental and numerical study is presented to investigate the effect of a crack embedded in the continuous adherend at an overlap end on failure behavior of an adhesive-bonded composite lap shear joint. In the experimental part, illustrated are the effect of the crack length on failure mechanism and loads. It is found that the presence of a crack at the overlap end can significantly reduce the static failure loads of the lap shear joints. For example, the failure load of a joint with a 10 mm long crack can be decreased by up to 44% comparing to that of the non-cracked one. Finite element method is then used to study the effect of the crack on both peel and shear stress distributions in the adhesive layer. The mode I and II energy release rates are also calculated using the virtual crack closure integral method, and then used to interpret the failure mechanism.

KEYWORDS: damage tolerance, crack, energy release rate, failure mechanism, failure load, lap shear joint.

INTRODUCTION

It is well known that damage tolerance is one of the major issues in application of advanced laminated composite structures. This is because such types of composite structures are prone to impact damage, which usually exists in a form of delamination between plies. Although there exist a large amount of research work addressing damage tolerance of stiffened panels, there has been no little effort being devoted to addressing damage tolerance of bonded composite stiffened panels, in which delamination occurs between several plies right at stiffener or flange ends [1-4]. It is known that interlaminar delamination is a typical failure mode observed in an adhesive-bonded composite lap joint [5]. The two major contributing factors are considered to be the high gradient of peel stress at overlap ends and the interlaminar weakness of composite adherents. Thus it is desirable to know the effect of delamination or interlaminar crack on the failure load and failure mechanism of bonded laminated composite structures. Investigation of such effect not only can provide us with an alternative method for predicting joint strength but also can be used as a basis for investigation of damage tolerance of adhesive-bonded composite structures. In doing so, an

adhesive-bonded composite lap-shear joint subjected to an axial load is considered. The objective of this study is to investigate the effect of an embedded crack on the stress distributions in adhesive layer, and the failure load and mechanism of adhesive-bonded composite lap shear joints. Experimental results reveal that the failure load can be significantly reduced due to the presence of an embedded crack at the chosen location and the failure mechanism can be completely changed as comparing to that of a virgin joint. A finite element analysis is presented to study the effect of crack size on the peel and shear stress distributions in the adhesive layer as well as on mode I and II energy release rates.

EXPERIMENTAL INVESTIGATION

Specimen Preparation and Testing Procedure

Figure 1 shows the major dimensions of the testing section of the lap shear joint specimens. All specimens have the same width of 25.4mm, the same adherent thickness of 1.72 mm and the same bondline thickness of 0.16 mm. For all specimens, the cracks were embedded between the surface and the second ply 0.215 mm beneath the surface. The crack length is varied from 0 to 10 mm. There are five specimen groups, LSJ-0, LSJ-2, LSJ-4, LSJ-8 and LSJ-10, in which the last digit indicates the crack length. For example, LSJ-4 represents a specimen with an embedded crack of 4 mm long, while LSJ-0 represents the virgin specimen.

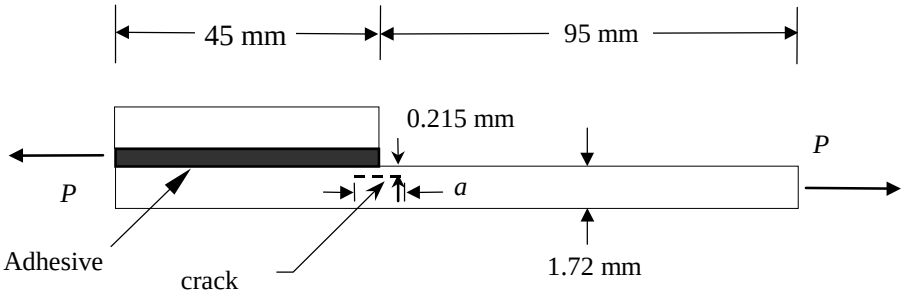

Figure 1: Dimensions of the lap shear joint specimens
(clamping sections at both ends are not shown in the figure).

As described in Tong [3], the material used was T300/934 carbon/epoxy plain woven prepreg, which has a curing temperature of 177°C and possesses the same mechanical properties in both warp and weft directions. Composite panels were manufactured by laminating 8 plies of the plain-woven prepreg in 0° direction, i.e. $(0)_{8S}$. Each ply had a nominal thickness of 0.215 mm. All panels were then cured in an autoclave following the curing cycle recommended by manufacturer [6]. In the lay-up process, two plies of 0.02 mm thick Teflon film of different width were embedded between the surface and second ply to introduce the crack of different length at the chosen location shown in Figure 1. It is worth pointing out that although the use of Teflon film to model cracks is a common practice, it can be argued that such a practice tends to form a notch rather than a sharp crack. In the curing process, care must be taken to ensure that all the Teflon films stay at the right position. FM300-K film adhesive was then used to bond the two panels following a moderate hand sanding with sandpaper and an acetone wash. Metal shims were used to achieve a uniform bondline thickness of 0.16 mm. Specimens were prepared by cutting the panels in such a way that there were no metal shims

left in the bonding area. Aluminum end taps of size 25.4 mm by 40 mm were used to overcome the eccentricity introduced when installing a specimen on testing machine.

All specimens were loaded in axial tension on an Instron testing machine at a loading rate of 0.5 mm/min. The applied load and the cross-head displacement were recorded.

Experimental Results and Discussion

For the specimens with no crack, the applied load increases linearly with the crosshead displacement until the ultimate sectional fracture as shown in Figure 2(a). For the specimens with an embedded crack, it was noted that at least one load drop took places prior to the final sectional failure. In-situ microscopic inspection revealed that crack propagation and onset of delamination at the crack tip inside the overlap caused such load drop. However, unlike the case of single-lap joints [3], such crack propagation arrests instead of leading to a catastrophic delamination. Further increase in the applied force causes further stable development of delamination at both crack tips within and outside of the overlap, accompanied by several load drops before the ultimate cross sectional failure as depicted in Figure 1(b). Microscopic inspection revealed that the crack propagated in a wavy manner possibly due to the woven nature of each ply, and the travel distance of internal crack tip is much larger than that of the external crack tip as schematically shown in Figure 2(b).

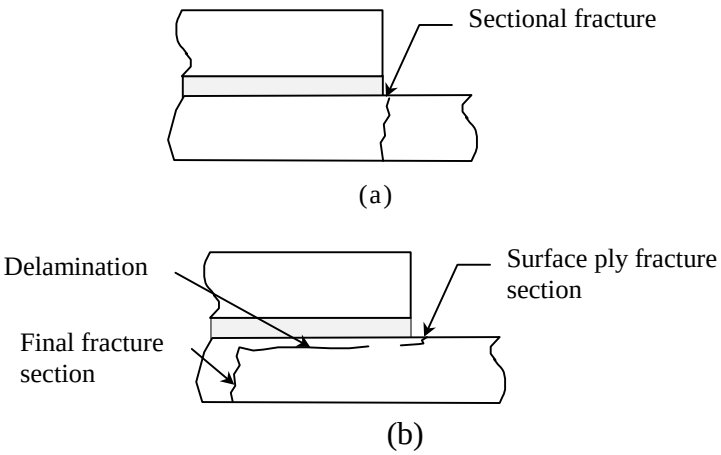

Figure 2: Typical fracture modes (a) LSJ-0 and (b) LSJ-2, LSJ-4, LSJ-8 and LSJ-10.

Table 1. Failure loads of specimen group LSJ-0 without embedded crack

Specimen	Failure load (kN)	Failure displacement (mm)
LSJ-0-1	19.162	3.483
LSJ-0-2	18.272	3.195
LSJ-0-3	17.502	2.97
LSJ-0-4	18.987	3.216
LSJ-0-5	18.765	3.375
LSJ-0-6	19.048	3.393
LSJ-0-7	17.105	2.935
Average	18.406±0.814	3.224±0.211

Tables 1-5 list the average failure loads, the average values of the first load drop and the average failure displacements. Evidently, the presence of embedded crack causes a significant reduction in the average failure load, i.e. 31%, 34%, 37% and 44% reduction in the average

failure load for the joints with a crack length of 2, 4, 8 and 10 mm, respectively, comparing to that of a virgin specimen. The standard deviation for the failure load is relatively consistent of the value about 0.8 except for specimen LSJ-4 which is 1.787. The results indicate that the failure displacement decreases as the crack length is increased from 0 to 10 mm. Comparing to virgin specimen, reduction in the failure displacement is 26%, 32%, 35% and 41%, respectively, for specimens with a crack of 2, 4, 8 and 10 mm respectively. The average value of the first load drop seems to be large for specimens with a short initial crack of 2 and 4 mm long and tends to be small for those with a long initial crack of 8 and 10 mm.

Table 2. Failure loads of specimen group SLJ-2 with embedded crack of 2 mm long

Specimen	Failure load (kN)	1st load drop (kN)	Failure displacement (mm)
LSJ-2-1	12.182	0.205	2.317
LSJ-2-2	12.083	0.409	2.313
LSJ-2-3	13.376	0.842	2.545
LSJ-2-4	13.707	1.001	2.479
LSJ-2-5	12.062	0.474	2.258
Average	12.682±0.794	0.5862±0.327	2.3824±0.123

Table 3. Failure loads of specimen group SLJ-4 with embedded crack of 4 mm long

Specimen	Failure load (kN)	1st load drop (kN)	Failure displacement (mm)
LSJ-4-1	14.505	1.546	2.455
LSJ-4-2	10.989	0.005	2.322
LSJ-4-3	10.51	0.17	1.978
LSJ-4-4	12.294	0.682	2.033
Average	12.074±1.787	0.601±0.693	2.197±0.229

Table 4. Failure loads of specimen group LSJ-8 with embedded crack of 8 mm long

Specimen	Failure load (kN)	1st load drop (kN)	Failure displacement (mm)
LSJ-8-1	12.728	0.482	2.528
LSJ-8-2	11.065	0.43	2.038
LSJ-8-3	11.879	0.3	2.082
LSJ-8-4	11.274	0.32	2.128
LSJ-8-5	11.393	0.297	2.226
LSJ-8-6	12.382	0.357	2.202
LSJ-8-7	12.476	0.568	2.31
LSJ-8-8	10.493	0.23	1.978
LSJ-8-9	10.660	0.23	1.447
Average	11.594±0.812	0.357±0.123	2.104±0.296

Table 5. Failure loads of specimen group LSJ-10 with embedded crack of 10 mm long

Specimen	Failure load (kN)	1st load drop (kN)	Failure displacement (mm)
LSJ-10-1	9.791	0.29	1.79
LSJ-10-2	10.531	0.346	1.998
LSJ-10-3	10.878	0.497	2.13
LSJ-10-4	10.14	0.31	1.883
LSJ-10-5	11.119	0.43	2.462
LSJ-10-6	10.284	0.49	1.528
LSJ-10-7	11.089	0.404	2.143
LSJ-10-8	8.991	0.345	1.323
Average	10.353±0.723	0.389±0.0.079	1.907±0.363

Figure 3 plots the measured average failure loads versus the crack length for the lap shear joint specimens. For the sake of comparison, the average measured failure loads of single lap joints [3] are also shown in this figure. It is evidently shown that the lap shear joint configuration is more sensitive to the embedded crack at the chosen location than the single lap joint configuration.

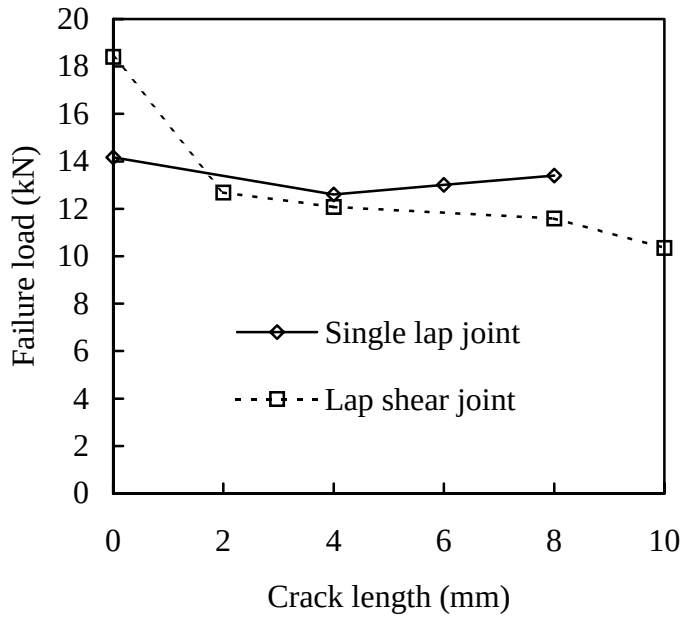

Figure 3: Effect of crack length on failure load of single lap and lap shear joints.

FINITE ELEMENT ANALYSIS

FEA Modeling

A 2-D plane strain finite element analysis procedure was used to model the behavior of adhesive-bonded lap shear joint specimens with and without cracks using Strand 6 [7]. In the analyses, all materials were assumed to be linearly elastic and finite deformation was not included. All dimensions for each specimen configuration has been given in detail in Figure 1 and the previous section. The mechanical properties for a single woven ply of T300/934 composites are given in Tables 6 [3,8], and Table 7 tabulates the Young's modulus and the Poisson's ratio for FM300K film adhesive [3].

Table 6: Mechanical properties of a single cloth ply.

Longitudinal modulus E_1=E_2 (MPa)	57226
Transverse modulus E_3 (MPa)	4800
In-plane shear modulus G_{12} (MPa)	4481
Out-of-plane shear modulus G_{13}=G_{23} (MPa)	4400
In-plane Poisson ratio μ_{12}	0.05
Out-of-plane Poisson ratio μ_{13}=μ_{23}	0.28

Table 7: Properties of FM300-K film adhesive.

Young's modulus E (MPa)	2400
Poisson ratio μ	0.32

Four-node quadrilateral plane strain elements were used to model the adherends and the adhesive layer. To mesh the joint specimens, one element was used for each ply and the adhesive layer in the through-the-thickness direction. Fine mesh with elements of 0.2121 mm long was adopted near overlap ends and cracks tips and coarse mesh with elements of up to 1 mm long was used in the remaining areas. Three elements across the adherend thickness were used for the surface and second plies between the crack tips. Small rectangular elements (0.0707 by 0.0667 mm) were used in the vicinities of the crack tips as sketched in Figure 4.

Five finite element models were generated to model all specimens with and without embedded cracks. At the left end of the specimen, namely x=0 (see Figure 4), displacements in both x and y directions are not allowed, while at the right end of the specimen, namely x=140 mm, vertical displacement is disabled. Constraint conditions are introduced to impose uniform displacement in the x direction at the right end of the all specimen. A uniform stress of 450 MPa is applied at the end of x=140 mm.

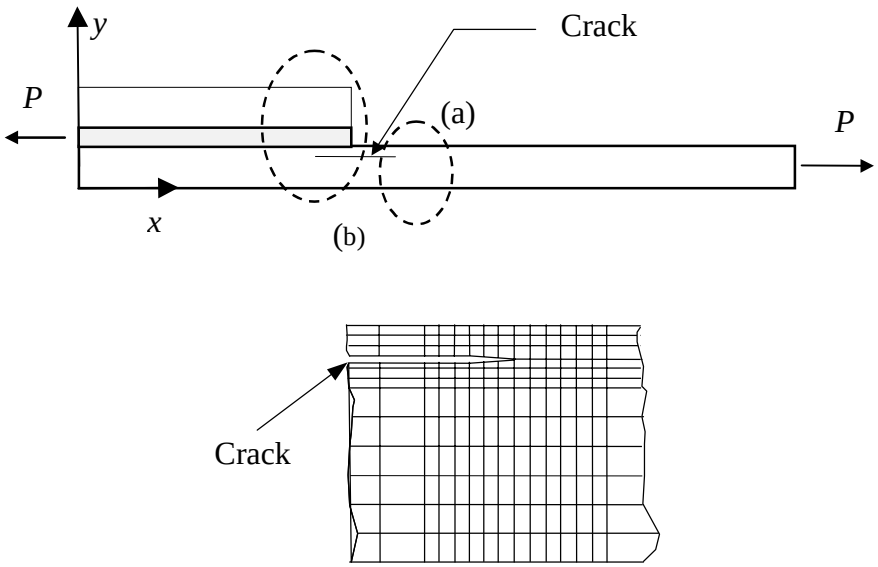

(a) A sketch of the mesh used near crack tip outside the overlap

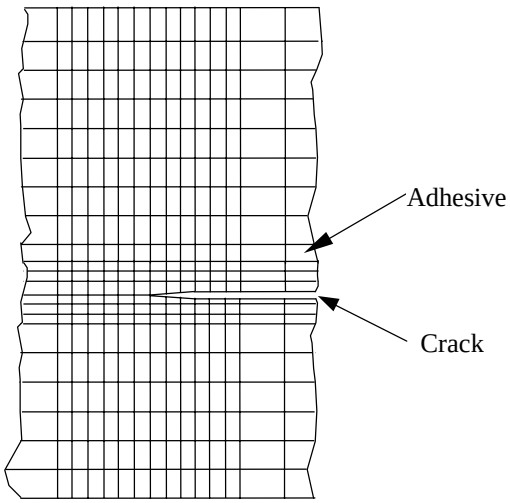

(b) A sketch of the mesh used near crack tip within the overlap

Figure 4: Sketches of the mesh used near the crack tips inside and outside the overlap.

Numerical Results and Discussion

Figures 6 and 7 depict the shear and peel stress distributions in the adhesive layer along the x direction for the lap shear joints with no crack and with a crack of 2, 4, 8 and 10 mm long respectively. All stresses are taken from the values at the center of each adhesive element. It is found that there exists another stress concentration in the adhesive layer at the internal crack tip in addition to the adhesive end when the crack is present.

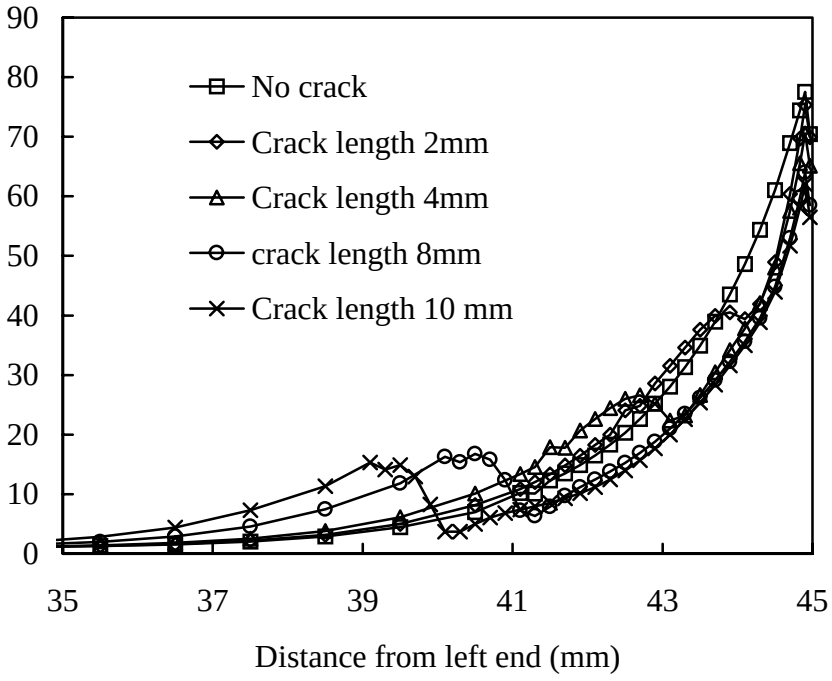

Figure 5: Effect of crack size on the shear stress distribution.

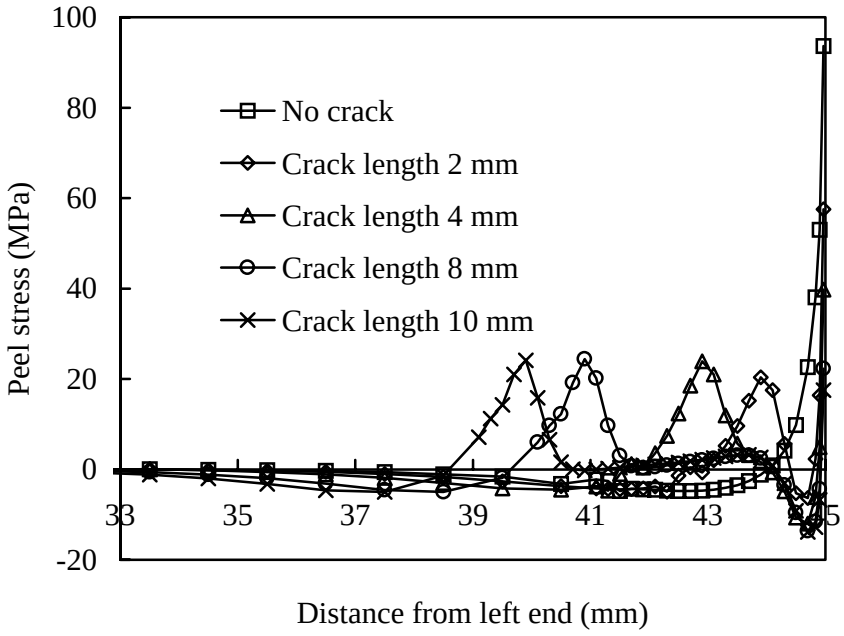

Figure 6: Effect of crack size on the peel stress distribution.

Existence of the second stress concentration alleviates the stress concentration at the adhesive end. Comparing to the virgin specimen, the presence of a crack can significantly reduce the peak peel stress at the adhesive end and can slightly decrease the peak shear stress. This is demonstrated by Figure 7 in which the non-dimensional peel and shear stresses, defined as the peak stress of a cracked specimen divided by that of a virgin specimen, are plotted versus the crack length. Figure 6 also shows that the peak peel stress in the adhesive layer near the internal crack tip takes the value of 20.4, 23.9, 24.5 and 24.1 MPa respectively for the cracked joints with a crack of 2, 4, 8 and 10 mm long. This clearly indicates that the location of the second peel stress concentration travels with the propagating internal crack tip. For relatively long crack, the peak peel stress near the internal crack tip becomes larger than that at the adhesive end, for example 24.5 versus 22.3 MPa, and 24.1 versus 17.5 MPa for joints with a crack of 8 and 10 mm long, respectively. It is believed that the peak peel and shear stresses near the internal crack tip are one of the major contributing factors to the crack propagation and arrest.

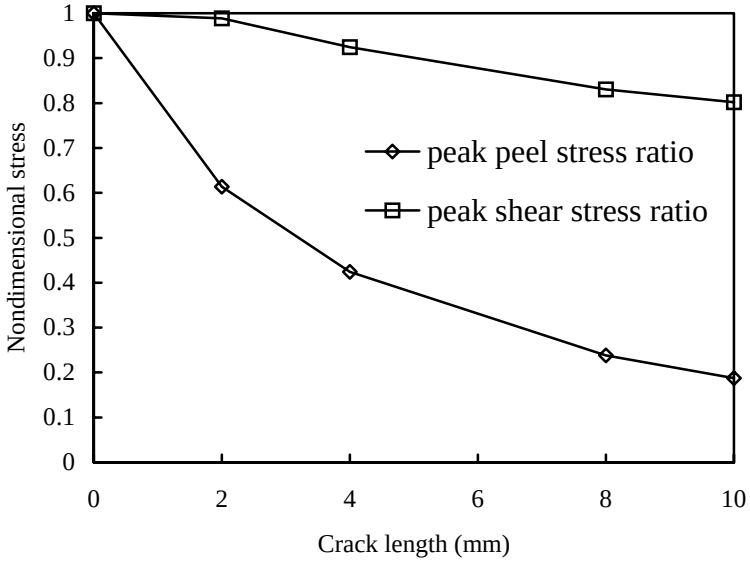

Figure 7: Effect of crack length on the peak peel and shear stresses at the adhesive end.

Figures 8 and 9 plot the mode I and II energy release rates versus the half crack length calculated at both crack tips inside and outside of the joint overlap. The energy release rates were calculated using the virtual crack closure method [9]. It is seen that the mode I energy release rate at the internal crack tip is significantly larger than that at the external crack tip. When the half crack length is enlarged from 1 to 5 mm, the energy release rate of mode I increases only slightly while that of mode II decreases dramatically. For the energy release rate of mode II, its value at the external crack tip is significantly larger than that at the internal crack tip. However, as the crack becomes longer, the energy release rate of mode II at both crack tips coincides and seems to approach to a constant. It is seen that at the internal crack tip the mode I deformation is dominant for the short crack case only and the mixed mode deformation becomes predominant for relatively long crack. At the external crack tip, the mixed mode deformation is predominant for the short crack cases while the mode II deformation is imperative for long crack cases. As for most engineering materials, the energy release rates of mode I are generally larger than those of mode II. Thus it is evident that the internal crack tip is more critical than the external one, and thus crack propagation will predominantly take place in a manner of internal crack propagation. This is in agreement with the experimental observation as schematically shown in Figure 2(b). This result is also

similar to that observed and predicted for the case of a single lap joint with two embedded cracks [3]. However, it is not clear from the present numerical results why a stable crack propagation takes place in a cracked lap shear joint rather than a catastrophic one as observed in a cracked single lap joint. One major contributing factor could be due to the clamped boundary condition at the left end (x=0 mm), which eliminates free rotation of the overlap occurring in single lap joint and thus arresting the crack propagation towards the left end. Another factor could be that the finite deformation and nonlinear material properties should be included in the analysis in order to better calculate the energy release rates and to predict the failure loads of the lap shear joints with and without embedded cracks.

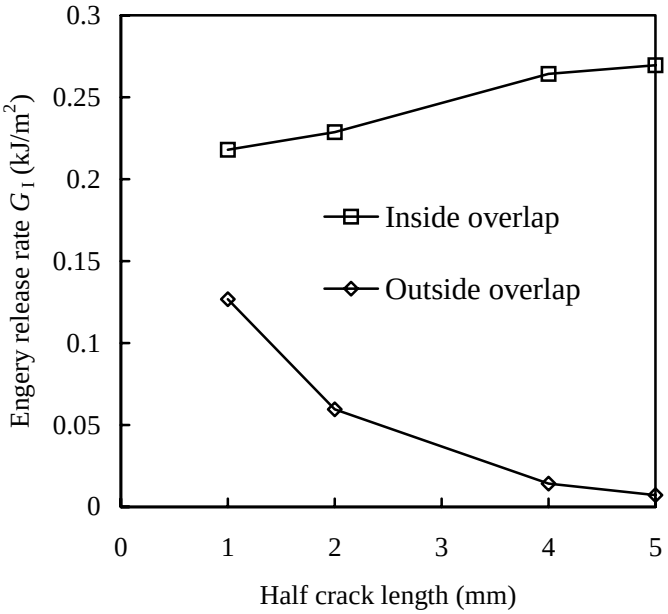

Figure 8: Mode I energy release rate at crack tips inside and outside the overlap.

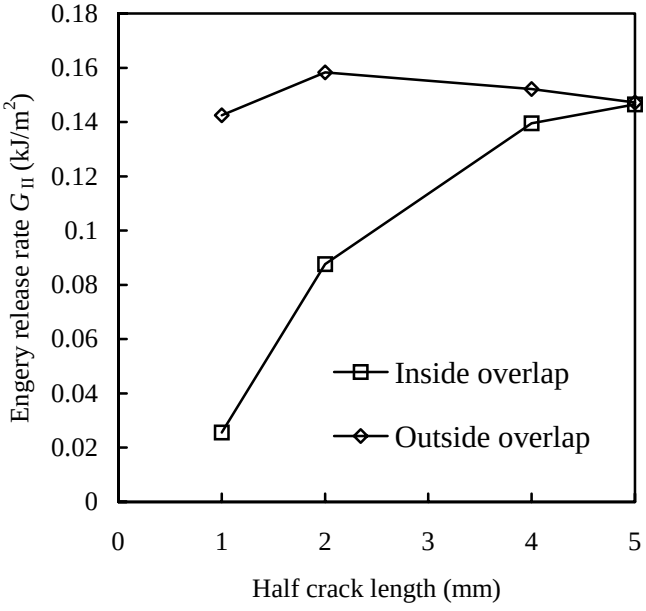

Figure 9: Mode II energy release rate at crack tips inside and outside the overlap.

CONCLUDING SUMMARY

An experimental and numerical study was carried out to investigate the effect of a crack embedded in the continuous adherent near the overlap end on failure behavior of an adhesive-bonded composite lap shear joint. Experimental results show that the existence of the crack at the chosen location can significantly reduce the static failure strength comparing with that of a virgin specimen. Testing results indicate that the internal crack tip propagates towards the clamped end of the joints prior to the ultimate sectional fracture near the clamped end. The numerical results obtained using linear analysis shows that the crack tip within the overlap is more critical than that outside the overlap. Further research is in progress to include finite deformation and nonlinear material effect to better predict the failure behavior of the cracked lap shear joints.

REFERENCES

1. Madan R.C., Walker B.A. and Murphy M.F., «Impact damage analysis for composite multistringer bonded panels», *Advanced Composites III: Expanding the Technology*, Proceedings of the 3rd Annual Conference on Advanced Composites, 15-17 September 1987, Detroit, Michigan, USA, pp. 43-51.

2. Tong L., Zhu X. & Steven G.P., «Damage tolerance of adhesively bonded composite joints», *Key Engineering Materials*, Vol. 145-149 (1998) pp. 537-542.

3. Tong L. «Failure of adhesive-bonded composite single lap joints with embedded cracks», *AIAA Journal* Vol 36, No. 3 (1998), pp. 448-456.

4. Tong L. and Steven G.P. *Analysis and Design of Structural Bonded Joints*, Kluwer Academic Publisher, April 1999.

5. Adams RD, «Strength prediction for lap joints, especially with composite adherends: a review», *Journal of Adhesion*, Vol. 30 (1989), pp. 219-242.

6. Anonymous, *ICI Fiberite Materials Handbook*, Tempe, Arizona, USA, March 1989.

7. G+D Computing, *Strand6 - finite element analysis system*, September 1996, Sydney, Australia.

8. Anonymous, *Boeing Advanced Composites Handbook*, Seattle, Washington, USA, June 1986.

9. Rybicki E. F. & Kanninen M. F. «A finite element calculation of stress intensity factors by a modified crack closure integral», *Engineering Fracture Mechanics*, Vol. 9, 1977, pp. 931-938.